

# Terahertz quantum cascade VECSEL with watt-level output power

Cite as: Appl. Phys. Lett. **113**, 011104 (2018); <https://doi.org/10.1063/1.5033910>

Submitted: 06 April 2018 • Accepted: 20 June 2018 • Published Online: 02 July 2018

Christopher A. Curwen, John L. Reno and  Benjamin S. Williams



View Online



Export Citation



CrossMark

## ARTICLES YOU MAY BE INTERESTED IN

[High performance terahertz metasurface quantum-cascade VECSEL with an intra-cryostat cavity](#)

Applied Physics Letters **111**, 101101 (2017); <https://doi.org/10.1063/1.4993600>

[Thermoelectrically cooled THz quantum cascade laser operating up to 210 K](#)

Applied Physics Letters **115**, 010601 (2019); <https://doi.org/10.1063/1.5110305>

[Metasurface external cavity laser](#)

Applied Physics Letters **107**, 221105 (2015); <https://doi.org/10.1063/1.4936887>



Webinar  
Quantum Material Characterization  
for Streamlined Qubit Development

 Zurich  
Instruments

[Register now](#)

# Terahertz quantum cascade VECSEL with watt-level output power

Christopher A. Curwen,<sup>1,a)</sup> John L. Reno,<sup>2</sup> and Benjamin S. Williams<sup>1</sup>

<sup>1</sup>*Department of Electrical and Computer Engineering, University of California, Los Angeles, California 90095, USA*

<sup>2</sup>*Sandia National Laboratories, Center of Integrated Nanotechnologies, MS 1303, Albuquerque, New Mexico 87185, USA*

(Received 6 April 2018; accepted 20 June 2018; published online 2 July 2018)

We report a terahertz quantum-cascade vertical-external-cavity surface-emitting laser (QC-VECSEL) whose output power is scaled up to watt-level by using an amplifying metasurface designed for increased power density. The metasurface is composed of a subwavelength array of metal-metal waveguide antenna-coupled sub-cavities loaded with a terahertz quantum-cascade gain material. Unlike previously demonstrated THz QC-VECSELs, the sub-cavities operate on their third-order lateral modal resonance (TM<sub>03</sub>), instead of their first-order (TM<sub>01</sub>) resonance. This results in a metasurface with a higher spatial density of the gain material, leading to an increased output power per metasurface area. In pulsed mode operation, peak THz output powers up to 830 mW at 77 K and 1.35 W at 6 K are observed, while a single-mode spectrum and a low divergence beam pattern are maintained. In addition, piezoelectric control of the cavity length allows approximately 50 GHz of continuous, single-mode tuning without a significant effect on output power or beam quality. *Published by AIP Publishing.* <https://doi.org/10.1063/1.5033910>

Terahertz quantum-cascade (QC) lasers have emerged as a promising source of high-power, coherent terahertz radiation.<sup>1</sup> There are two existing methods for waveguiding in THz QC-lasers. The first is the surface plasmon (SP) waveguide,<sup>2</sup> in which the multiple-quantum-well gain material is grown above a highly doped semiconductor layer on a semi-insulating substrate which supports a loosely confined surface-plasmon mode. The second is the metal-metal waveguide,<sup>3</sup> in which the gain material is sandwiched between two metal layers to create a set of highly confined modes with sub-wavelength transverse dimensions. Multi-watt power levels have been demonstrated from SP waveguides; however, such high-power devices typically oscillate in multiple modes, have limited beam quality often with significant sidelobes, and have limited tunability.<sup>4–8</sup> THz QC-lasers based on metal-metal waveguides exhibit improved temperature performance over SP waveguides but suffer from even worse beam patterns and low outcoupling efficiency due to impedance mismatch and strong diffraction from their sub-wavelength radiating facets.<sup>9</sup> Metal-metal waveguide deficiencies have been greatly improved upon using a variety of design techniques such as distributed-feedback surface-emitting or end-fire cavities, photonic crystals, and antenna-coupled cavities, but so far, none of these solutions have been scalable to watt-level output powers.<sup>10–13</sup> In recent years, an alternative architecture has been demonstrated by building THz QC-lasers in a vertical-external-cavity surface-emitting laser (VECSEL) configuration.<sup>14</sup> Such devices have been demonstrated to lase in single-mode with near-diffraction-limited Gaussian output beams, peak pulsed powers over 100 mW, and continuous wave powers over 5 mW at 77 K.<sup>15–17</sup>

The enabling component of the THz QC-VECSEL is an amplifying reflectarray metasurface. In its simplest form, it consists of an array of narrow metal-metal waveguide ridges,

whose widths  $w$  are determined by the first-order resonance condition at the intended wavelength according to  $w \approx \lambda_0/2n$  ( $n$  being the index of refraction within the semiconductor). These ridges act as low-quality-factor sub-cavities that couple to the master high-Q external-cavity mode. The structure of each sub-cavity is similar in form to an elongated patch antenna, in which the transverse electric-field  $\vec{E}$  from each waveguide sidewall radiates according to equivalent magnetic current sources  $\vec{M}_s = 2\hat{n} \times \vec{E}$ , where  $\hat{n}$  is the surface normal.<sup>18,19</sup> Although the  $E_y$  field for the TM<sub>01</sub> mode is odd,  $\hat{n}$  is also odd so that the sidewall magnetic currents  $\vec{M}_s$  are in-phase for efficient surface normal radiation. In this letter, we introduce a metasurface design in which the metal-metal ridges are resonant in the TM<sub>03</sub> lateral mode. The transverse field  $E_y$  has the same symmetry and therefore couples to surface incident radiation in the same manner as the TM<sub>01</sub> ridges [see Figs. 1(a) and 1(b)]. However, because the TM<sub>03</sub> ridges are approximately three times as wide as the TM<sub>01</sub> ridges for a given frequency, we increase the amount of gain material (and injection current) per unit area. This increased “fill factor” allows us to greatly increase the VECSEL output power without having to increase the overall dimensions of the metasurface and allows for more efficient use of the epitaxially grown wafer.

The TM<sub>03</sub> metasurface was designed for operation at 3.4 THz using a finite-element electromagnetic solver. A single period of the metasurface structure was modeled in COMSOL Multiphysics with periodic boundary conditions, including losses within the metal and active region (see Ref. 15). The effect of a generic intersubband gain (equivalent to a frequency independent gain coefficient of 40 cm<sup>−1</sup>) was included via an anisotropic permittivity (see Ref. 14). In Fig. 2, the simulated reflectance of a TM<sub>01</sub> metasurface with a period  $\Lambda = 70 \mu\text{m}$  and ridge width  $w = 11.5 \mu\text{m}$  (fill factor = 0.16) is compared to a TM<sub>03</sub> metasurface with a period  $\Lambda = 70 \mu\text{m}$  and ridge width  $w = 36.3 \mu\text{m}$  (fill factor = 0.52).

<sup>a)</sup>Author to whom correspondence should be addressed: ccurwen@ucla.edu

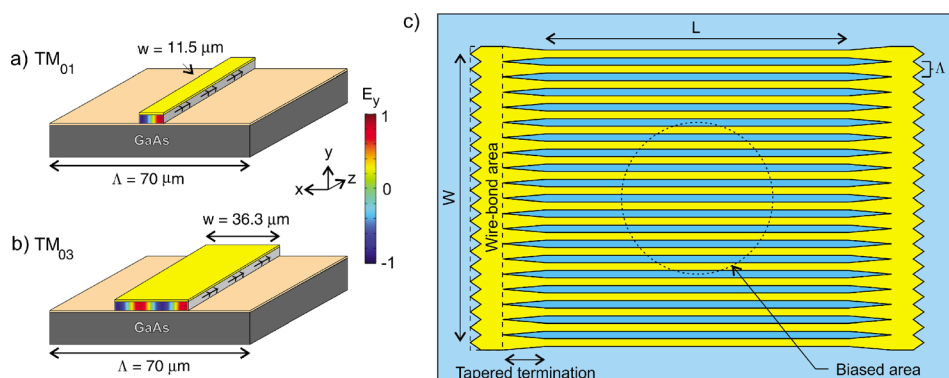


FIG. 1. Cross-sectional schematic of the metasurface unit cell that illustrates the difference between (a)  $TM_{01}$  and (b)  $TM_{03}$  metasurface designs. (c) Areal view of the  $TM_{03}$  metasurface.  $W=L=3$  mm for fabricated devices and bias area diameter = 1.5 mm. The tapered terminations are  $300\text{ }\mu\text{m}$  long, and each wire bond area is another  $300\text{ }\mu\text{m}$  in length, making the total length of the metasurface 4.2 mm.

The two curves are quite comparable, and in fact, the  $TM_{03}$  metasurface gives slightly higher reflectance. In principle, a similar increase in the fill factor could be accomplished with a  $TM_{01}$  design by simply reducing the period  $\Lambda$ . However, simulation results in Fig. 2 (dotted line) show that simply reducing the period of the  $TM_{01}$  structure ( $\Lambda = 24\text{ }\mu\text{m}$ ,  $w = 12.5\text{ }\mu\text{m}$ , and fill factor = 0.52) leads to much stronger coupling between neighboring ridges, which results in a metasurface with a much weaker peak reflectance. This broader resonant response corresponds to reduced field enhancement within the ridges. While this is not inherently bad, it makes the VECSEL more sensitive to any source of loss from the external cavity.<sup>15</sup>

$TM_{03}$  metasurface devices were fabricated using the standard metal-metal (Cu-Cu) waveguide microfabrication techniques outlined in Refs. 14 and 20. The metasurface selected for testing was a  $3 \times 3\text{ mm}^2$  metasurface with tapered terminations leading to wire-bonding areas. By selectively depositing silicon dioxide between the GaAs/AlGaAs QC-laser material and the top Ti/Au metal contact, we electrically bias only a center circular area of 1.5 mm diameter in order to preferentially pump the fundamental transverse cavity mode. The  $10\text{ }\mu\text{m}$  thick active region is grown by molecular beam epitaxy and is based on the hybrid resonant-phonon/bound-to-continuum design concept;<sup>21</sup> it is the same design used by Li *et al.* in Ref. 4, and it is the same wafer as used in Refs. 15 and 16 (wafer VB0739). The

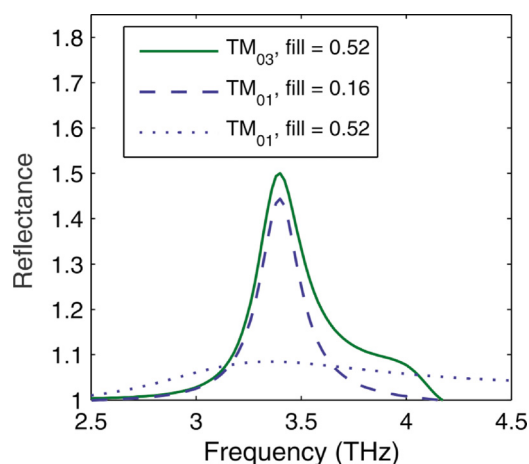


FIG. 2. Simulated reflectances for several metasurfaces when  $40\text{ cm}^{-1}$  of intersubband gain is applied. Comparison is made between  $70\text{ }\mu\text{m}$  period  $TM_{03}$  and  $TM_{01}$  surfaces, as well as a high fill factor  $TM_{01}$  surface with a  $24\text{ }\mu\text{m}$  period.

output couplers used were inductive and capacitive metal-meshes deposited on a  $135\text{ }\mu\text{m}$  thick z-cut quartz substrate (see [supplementary material](#) Fig. S1). Both the metasurface and the output coupler were mounted inside the cryostat. This removes any windows from within the external cavity, as in Ref. 16. Also, in this work, we have added the ability to tune the length of the external cavity *in situ* by mounting the output coupler on a piezoelectric stepping stage (see [supplementary material](#) Fig. S2).

The results using an inductive mesh output coupler with  $\sim 9\%$  transmission (OC1) are plotted in Fig. 3. All measurements reported here were taken in the pulsed mode (550 ns pulses at a 2 kHz repetition rate) as the large power dissipation prevents continuous-wave operation. Power vs. current ( $P$ - $I$ ) curves were measured with a pyroelectric detector (Gentec), and absolute power levels were measured using a calibrated thermopile. Peak power levels of 0.79 W and 1.1 W were measured at 77 K and 6 K, respectively, and the output intensity with current is observed to be very linear with slope efficiencies ( $dP/dI$ ) of 380 mW/A and 420 mW/A at 77 K and 6 K, respectively. The cryostat was equipped with a parylene anti-reflection coated high-resistivity silicon window whose measured transmission is  $\sim 90\%$  at 3.3 THz; the 10% window absorption has been accounted for in the reported power data. Spectra were measured using a Fourier-transform infrared (FTIR) spectrometer with a  $0.5\text{ cm}^{-1}$  resolution. By stepping the piezoelectric stage, continuous tuning of the laser frequency is observed from  $\sim 3.27$  to 3.32 THz. This 50 GHz tuning range is limited by the free spectral range (FSR) of the external cavity; as the lasing mode is tuned away from the lowest threshold point, the adjacent longitudinal mode is tuned closer to the lowest threshold point and eventually a mode hop occurs. The change in the cavity length as the VECSEL is tuned cannot be stated exactly as the piezoelectric stage is operated with an open-loop controller that does not have a position readout, but we can estimate its change since we know that the cavity length must change by half of a wavelength to hop back to the starting frequency. The cavity FSR can be used to estimate the cavity length ( $\sim 3$  mm long in this case), but the FTIR does not allow the FSR to be determined with sufficient resolution to state an exact cavity length. The VECSEL characteristics (threshold, slope efficiency, output power, etc.) are influenced not only by the gain spectrum of the QC-material but also by the spectral response of the metasurface and the reflectance of the output coupler. The reflectivity of

the output coupler is relatively flat through the tuning range (see [supplementary material Fig. S1](#)), as is the measured output power [Fig 3(b)] and threshold current (see [supplementary material Fig. S3](#)), which suggests that the QC-gain and the metasurface reflectance are also relatively constant through this range. A circular, high-quality beam with a full-width half-maximum divergence angle of  $\sim 4^\circ$  is consistently observed as the VECSEL is tuned (see [supplementary material Fig. S4](#) for Gaussian curve fitting to 1-D beam cuts). Two-axis beam measurements were performed using a 2-mm diameter pyroelectric detector scanned in a spherical pattern at a constant distance of 15 cm from the VECSEL ( $0.8^\circ$  resolution).

Next, in Fig. 4, we present the VECSEL's performance using the same  $\text{TM}_{03}$  metasurface, but using a lower reflectance capacitive mesh output coupler, measured to have  $\sim 18\%$  transmittance (OC2, see [supplementary material Fig. S1](#)). Threshold currents, slope efficiencies, and maximum

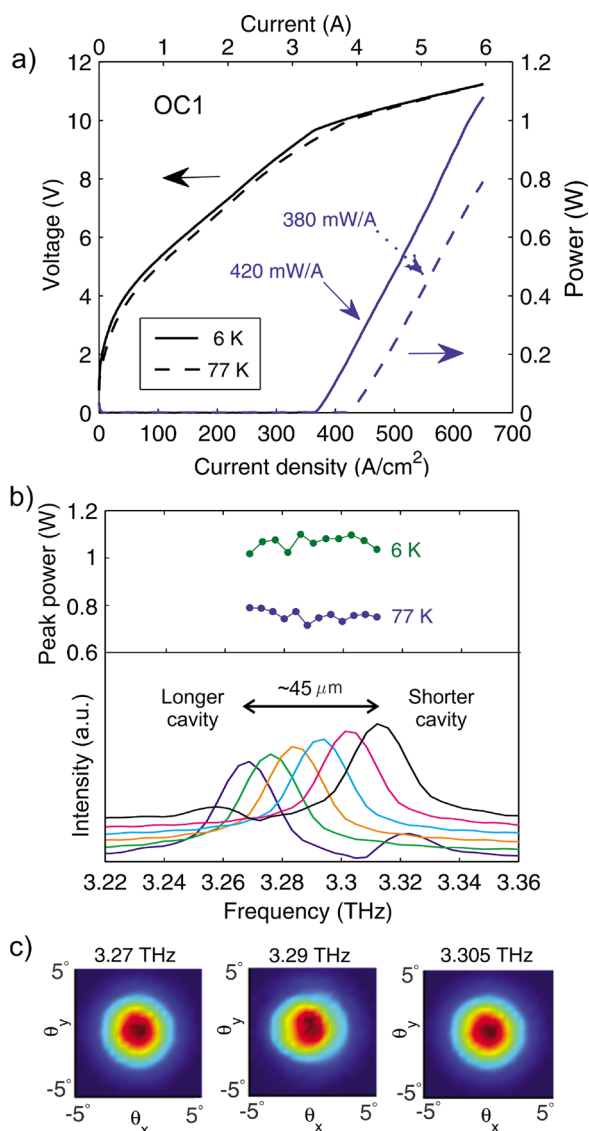


FIG. 3. (a) Pulsed-mode power and voltage vs. current characteristics from  $\text{TM}_{03}$  VECSEL using a highly reflective output coupler with a measured transmission of  $\sim 9\%$ . (b) Normalized Fourier-transform infrared (FTIR) spectra collected as the VECSEL cavity length is tuned via a piezoelectric stepping stage, and corresponding output power as a function of frequency at 77 K and 6 K. (c) VECSEL far-field beam patterns.

powers all increase at both 77 K and 6 K compared to when OC1 was used, which indicates that the laser is closer to the optimum outcoupling condition. A maximum peak power of  $\sim 1.35$  W and a peak slope efficiency of 767 mW/A are observed in a single mode with a narrow, Gaussian shaped beam and peak wall-plug efficiency of  $\sim 2\%$  at 6 K (see Fig. 5). The lasing frequency when using OC2 was  $\sim 3.38$  THz, slightly higher than OC1, which lased closer to 3.3 THz. This can be explained by observing that OC2 is more reflective at higher frequencies, which results in lower threshold currents at higher frequencies (see [supplementary material Fig. S1](#)). The VECSEL was again tuned through the cavity FSR of  $\sim 80$  GHz, from 3.31 to 3.39 THz (cavity length  $\sim 1.9$  mm); however, there is a strong atmospheric absorption line at  $\sim 3.335$  THz that makes it difficult to accurately characterize the power and slope efficiency as a function of tuning (see [supplementary material Fig. S6](#)). It is notable that the  $P$ - $I$  characteristic exhibits sub-linear behavior at higher injection currents (particularly at 6 K). This is not due to a heating effect, as short pulses are used, and no such sub-linear behavior is observed when using the same metasurface with OC1. We speculate that this sub-linear behavior may be due to the onset of additional lasing in propagating (i.e., guided) waveguide modes that do not radiate but still compete with the  $\text{TM}_{03}$  VECSEL mode for gain. Indeed, the metasurface is observed to “self-lase” even in the absence of an output coupler, albeit at threshold currents higher than required to lase in the VECSEL mode (see [supplementary material Fig. S7](#)). However, the simultaneous lasing of guided modes along with the VECSEL mode cannot be readily verified given the limited resolution and dynamic range of our FTIR spectrometer since the guided modes do not radiate significantly, and any scattered power would be indiscernible from the high power of the VECSEL mode. This problem could be remedied in the future by making the metasurface even larger compared to the bias area (i.e., a  $5 \times 5 \text{ mm}^2$  metasurface with a 1.5 mm bias diameter rather than a  $3 \times 3 \text{ mm}$  metasurface with a 1.5 mm bias diameter),

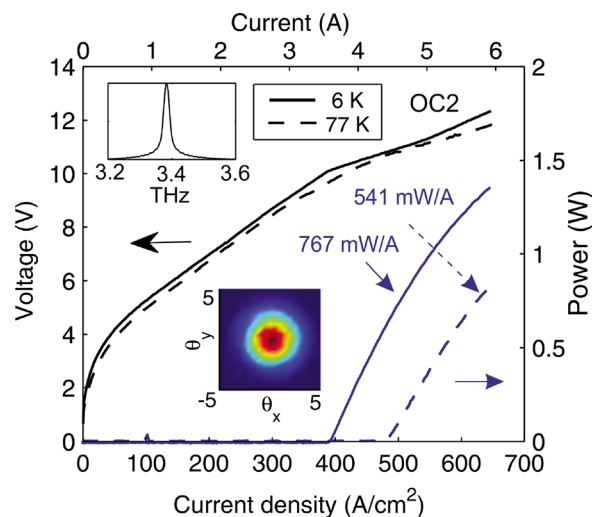


FIG. 4.  $P$ - $I$ - $V$  data from  $\text{TM}_{03}$  VECSEL using a low reflective output coupler with a measured transmission of  $\sim 18\%$ . Note that the on-chip voltage probe failed during experiment, so voltage data were measured outside of the cryostat (i.e., a two-terminal measurement) and scaled with a series resistance (see [supplementary material Fig. S5](#)).



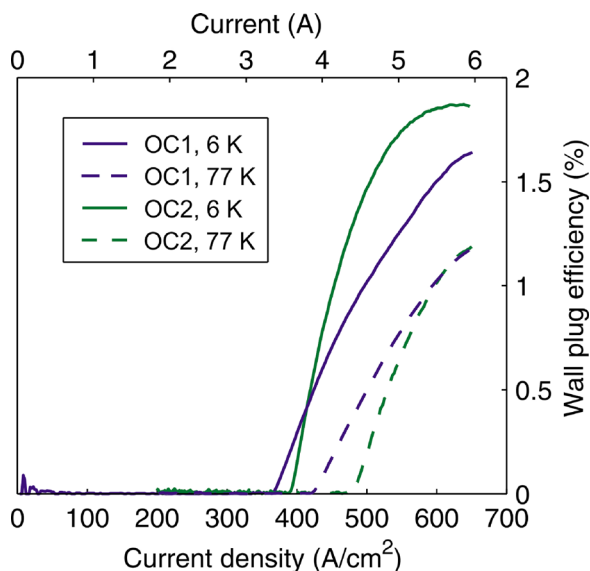


FIG. 5. Wall plug efficiency as a function of electrical pump power for the  $TM_{03}$  metasurface. Results for both OC1 and OC2 at 77 K and 6 K are presented.

so that the additional unbiased section would add more round-trip loss to the propagating modes. Alternatively, more loss could be added to the terminations by leaving a heavily doped GaAs contact layer exposed at the edges of the metal.<sup>22</sup>

In conclusion, we have demonstrated the use of the third-order lateral resonance of metal-metal ridge waveguides to increase the peak output power of a THz QC-VECSEL to above 1 W in the pulsed mode. A further increase in the THz QC-VECSEL power should be possible by making the metasurface even larger, or even moving to a  $TM_{05}$  resonant metasurface, should there be a need for such multi-watt level peak powers. However, our results suggest that increased efforts should be made in the future to suppress parasitic lasing of confined modes to prevent gain-competition and roll-over of the power-current characteristics. Additionally, by using piezoelectric intracavity control of the cavity length, we have shown the potential of the VECSEL cavity to provide modest single-mode tunability of 1%–2% without degrading the laser output power and while maintaining excellent beam quality.

See [supplementary material](#) for data on output couplers, illustrations of the VECSEL cavity construction, measurements of voltage-current characteristics, and additional data collected from the metasurface.

Microfabrication was performed at the UCLA Nanoelectronics Research Facility, and wire bonding was performed at the UCLA Center for High Frequency

Electronics. This work was performed, in part, at the Center for Integrated Nanotechnologies, an Office of Science User Facility operated for the U.S. Department of Energy (DOE) Office of Science. Sandia National Laboratories is a multimission laboratory managed and operated by National Technology and Engineering Solution of Sandia, LLC., a wholly owned subsidiary of Honeywell International, Inc., for the U.S. Department of Energy's National Nuclear Security Administration under Contract No. DE-NA-0003525. Partial funding was provided by the National Science Foundation (1407711 and 1711892) and National Aeronautics and Space Administration (NNX16AC73G).

- <sup>1</sup>M. S. Vitiello, G. Scalari, B. Williams, and P. De Natale, *Opt. Express* **23**(4), 5167 (2015).
- <sup>2</sup>R. Kohler, A. Tredicucci, F. Beltram, H. E. Beere, E. H. Linfield, A. G. Davies, D. A. Ritchie, R. C. Iotti, and F. Rossi, *Nature* **417**(6885), 156 (2002).
- <sup>3</sup>B. S. Williams, S. Kumar, H. Callebaut, Q. Hu, and J. L. Reno, *Appl. Phys. Lett.* **83**(11), 2124 (2003).
- <sup>4</sup>L. Li, L. Chen, J. X. Zhu, J. Freeman, P. Dean, A. Valavanis, A. G. Davies, and E. H. Linfield, *Electron. Lett.* **50**(4), 309 (2014).
- <sup>5</sup>L. Li, L. Chen, J. R. Freeman, M. Salih, P. Dean, A. G. Davies, and E. H. Linfield, *Electron. Lett.* **53**(12), 799 (2017).
- <sup>6</sup>H. Richter, N. Rothbart, and H. W. Hubers, *J. Infrared, Millimeter, Terahertz Waves* **35**(8), 686 (2014).
- <sup>7</sup>A. W. M. Lee, B. S. Williams, S. Kumar, Q. Hu, and J. L. Reno, *Opt. Lett.* **35**(7), 910 (2010).
- <sup>8</sup>S. Chakraborty, O. Marshall, C. W. Hsin, M. Khairuzzaman, H. Beere, and D. Ritchie, *Opt. Express* **20**(26), B306 (2012).
- <sup>9</sup>A. J. L. Adam, I. Kasalynas, J. N. Hovenier, T. O. Klaassen, J. R. Gao, E. E. Orlova, B. S. Williams, S. Kumar, Q. Hu, and J. L. Reno, *Appl. Phys. Lett.* **88**(15), 151105 (2006).
- <sup>10</sup>M. I. Amanti, M. Fischer, G. Scalari, M. Beck, and J. Faist, *Nat. Photonics* **3**(10), 586 (2009).
- <sup>11</sup>H. Zhang, L. A. Dunbar, G. Scalari, R. Houdre, and J. Faist, *Opt. Express* **15**(25), 16818 (2007).
- <sup>12</sup>Y. Chassagneux, R. Colombelli, W. Maineult, S. Barbieri, S. P. Khanna, E. H. Linfield, and A. G. Davies, *Appl. Phys. Lett.* **96**(3), 031104 (2010).
- <sup>13</sup>L. Bosco, C. Bonzon, K. Ohtani, M. Justen, M. Beck, and J. Faist, *Appl. Phys. Lett.* **109**(20), 201103 (2016).
- <sup>14</sup>L. Xu, C. A. Curwen, P. W. C. Hon, Q. S. Chen, T. Itoh, and B. S. Williams, *Appl. Phys. Lett.* **107**(22), 221105 (2015).
- <sup>15</sup>L. Xu, C. A. Curwen, D. Chen, J. L. Reno, T. Itoh, and B. S. Williams, *IEEE J. Sel. Top. Quantum Electron.* **23**(6), 1200512 (2017).
- <sup>16</sup>L. Xu, C. A. Curwen, J. L. Reno, and B. S. Williams, *Appl. Phys. Lett.* **111**(10), 101101 (2017).
- <sup>17</sup>L. Xu, D. Chen, T. Itoh, J. L. Reno, and B. S. Williams, *Opt. Express* **24**(21), 24117 (2016).
- <sup>18</sup>P. W. C. Hon, A. A. Tavallaei, Q. S. Chen, B. S. Williams, and T. Itoh, *IEEE Trans. Terahertz Sci. Technol.* **2**(3), 323 (2012).
- <sup>19</sup>C. A. Balanis, *Advanced Engineering Electromagnetics* (Wiley, New York, 1989), p. xx.
- <sup>20</sup>B. S. Williams, S. Kumar, Q. Hu, and J. L. Reno, *Opt. Express* **13**(9), 3331 (2005).
- <sup>21</sup>M. I. Amanti, G. Scalari, R. Terazzi, M. Fischer, M. Beck, J. Faist, A. Rudra, P. Gallo, and E. Kapon, *New J. Phys.* **11**, 125022 (2009).
- <sup>22</sup>Y. Chassagneux, R. Colombelli, W. Maineult, S. Barbieri, H. E. Beere, D. A. Ritchie, S. P. Khanna, E. H. Linfield, and A. G. Davies, *Nature* **457**(7226), 174 (2009).